Mechanisms on Accelerating Hydration of Alite Mixed with Inorganic Salts in Seawater and Characteristics of Hydration Products

Yanjie SUN, Yangyang ZHANG, Yamei CAI, Wing Lun LAM, Jian-Xin LU, Peiliang SHEN, Chi Sun POON*

Department of Civil and Environmental Engineering,

The Hong Kong Polytechnic University, Hung Hom, Kowloon, Hong Kong

Corresponding author email: cecspoon@polyu.edu.hk

Author information

Corresponding author

Chi Sun POON - Department of Civil and Environmental Engineering, The Hong Kong Polytechnic University, Hung Hom, Kowloon, Hong Kong; Email: cecspoon@polyu.edu.hk

Authors

Yanjie SUN - Department of Civil and Environmental Engineering, The Hong Kong Polytechnic University, Hung Hom, Kowloon, Hong Kong; Email: yanjie.sun@connect.polyu.hk

Yangyang ZHANG - Department of Civil and Environmental Engineering, The Hong Kong Polytechnic University, Hung Hom, Kowloon, Hong Kong; Email: yangyangzhang_dlut@hotmail.com

Yamei CAI - Department of Civil and Environmental Engineering, The Hong Kong Polytechnic University, Hung Hom, Kowloon, Hong Kong; Email: ya-mei.cai@connect.polyu.hk

Wing Lun LAM - Department of Civil and Environmental Engineering, The Hong Kong Polytechnic University, Hung Hom, Kowloon, Hong Kong; Email: wing-lun-alan.lam@connect.polyu.hk

Jian-Xin LU - Department of Civil and Environmental Engineering, The Hong Kong Polytechnic University, Hung Hom, Kowloon, Hong Kong; Email: louis.lu@connect.polyu.hk

Peiliang SHEN - Department of Civil and Environmental Engineering, The Hong Kong Polytechnic University, Hung Hom, Kowloon, Hong Kong; Email: peiliang.shen@polyu.edu.hk

Abstract

Interest in exploring the use of seawater as the mixing water for preparing concrete is increasing due to the lack of freshwater in some coastal regions and remote islands, where seawater is more accessible. However, up to now, the mechanism of accelerating effects of seawater on the hydration of portland cement (PC) remains unclear. In this study, alite, a major clinker phase in PC, was hydrated with common salt solutions (NaCl, Na_2SO_4 and $MgCl_2$) in seawater to explore the mechanism of acceleration. The heat release peaks of the salt-added systems shifted to an earlier hydration time with a higher peak value, which indicated the faster hydration rate of alite pastes compared to the DI water system. The addition of the single salts was found to increase the concentration of Ca species in solutions, contributing to the increased formation of Calcium-Silicate-Hydrates (C-S-H) and portlandite at early ages. In the Na_2SO_4 system, gypsum was the new hydration product, while brucite was formed in $MgCl_2$ systems, which caused the sharp decrease of Mg species in the solution. The morphology of the early formed C-S-H was changed with the addition of the salts, and the C-S-H were characterized as thinner and longer fibres. At later ages, the incorporation of the single salts lowered the polymerization degree of C-S-H, but no noticeable morphology change was observed.

Keywords: Seawater; Cement; Alite; Hydration; Single salt

Introduction

From 2013 to 2020, over 4 billion tonnes of cement was produced annually worldwide, making it one of the most consumed materials in human society.[1] During the processing of cement to concrete, freshwater is needed. However, with the increasing demand for construction projects, a freshwater shortage could be a problem, especially for regions like the Middle East, North Africa, and some remote islands.[2] To meet the water requirement in these regions, seawater is being considered as an alternative to freshwater.

In recent years, increasing interest has grown towards research on seawater concrete.[3-5] However, seawater use is limited in concrete applications due to its high chloride content, which can cause corrosion of steel bars,[6-8] which would have a deleterious effect on the mechanical properties of the reinforced concrete structures. However, with the introduction of fibre-reinforced polymer (FRP) as reinforcement, there may be opportunities to use seawater to produce reinforced concrete, according to recent research on the performance of FRP in seawater.[9] It was found that FRP had a better corrosion resistance to seawater than steel,[10-11] and showed no significant long-term durability reduction (mainly tensile strength) under saline environment compared to that under freshwater environment.[12] Apart from the reinforced structures, seawater can also be applied in plain concrete mixing, which can be traced to more than 2000 years ago.[13] That provides another evidence for the potential to adopt seawater as the concrete mixing water.

At present, a number of studies have focused on the mechanical properties and chloride immobilization of concrete prepared with seawater. [5, 14-17] However, only a limited amount of studies was focused on the hydration process and mechanism of cement in seawater. One of the most commonly conducted tests to assess the effect of seawater on cement pastes is the calorimetry test. Most test results showed that the hydration of cement at an early age is significantly accelerated by adopting seawater as the mixing water, which is indicated by the higher heat release within a shorter period than freshwater-based mixing cement pastes.[5, 14-15] As a result, the early-age strengths of the concrete mixed with seawater were also enhanced. However, few studies have tried to explore the mechanisms behind the acceleration in the process of hydration observed in seawater mixed cement systems. Li et al. tried to explain the accelerating mechanism with the dissolution theory based on a

geochemical approach. According to their research, the formation of Friedel's salt was considered to be the reason for the accelerated reaction of C_3A and C_4AF, as it would consume a large amount of calcium, aluminate, and ferrite in the pore solution. The acceleration of C_3S was also attributed to the presence of Cl^- in seawater. However, no further discussion was provided on the influence of other abundant ions in seawater.[18] Younis et al. attributed the accelerating effects to the existence of NaCl in seawater, which would react with $Ca(OH)_2$ to form $CaCl_2$, one of the main accelerating admixtures. However, the effects of other salts in seawater were not discussed.[14] Wang et al. stated that Cl^-, Ca^{2+}, Mg^{2+}, Na^+ and SO_4^{2-} in seawater contributed to the hydration of alite, which was the main phase in PC, so the hydration of PC was accelerated. But, no in-depth explanation was given.[5] Yassen et al. explored the effects of seawater on the morphology of hydration products of C_3S pastes. It was found that the addition of seawater contributed to the formation of gypsum with sharp rod-like morphology.[19] However, the research mainly focused on the effects of SO_4^{2-}, and the effects of each single salt in seawater were not further studied.

Since seawater is a complex system with a variety of inorganic and organic phases, researchers tried to simplify the effects of seawater by using single inorganic salt in their studies. A ranking of the effect of different cations and anions was proposed by Edwards et al.;[20] however, they did not explain the underlying mechanism of the accelerating effect. Chloride is the most abundant anion in seawater. Kondo et al.[21] indicated that chloride could control the dissolution of OH^- by affecting the precipitation rate of the cement hydration products. Another possible explanation of the acceleration effect was that the ions in seawater changed the structure of the early formed C-S-H layer around the cement particle, making it more flocculated. Through the loose structure of the layer, ion exchange became more accessible, and the reaction was expedited.[22] Nevertheless, the 'layer' theory has been proven to be a less plausible reason by some researchers since there was no direct evidence of forming a continuous layer on the surface of alite.[23-25] At least, it was not the only reason for the beginning and the ending of the induction period. Brown et al. studied the effect of Ca^{2+} on the hydration of C_3S, and concluded that the excessive Ca^{2+} in solution would promote the precipitation of $Ca(OH)_2$ and the hydration of C_3S.[26] However, their theory could not fully apply to explain the acceleration mechanism of seawater since the

concentration of Ca^{2+} in seawater was less than those of Na^{+} and Mg^{2+} in seawater. Thus, the mechanisms for the acceleration phenomenon is not yet fully understood and more fundamental work needed to be done.

This paper tries to provide a more in-depth understanding of the effects of seawater on cement hydration. A subsystem was first evaluated to simplify the complex compositions of PC and seawater by first limiting the study to single salt solutions and alite, which is the major clinker phase in PC.

Materials and methods

Materials

The alite used in this study was purchased from DMT Materials Technology Company, China. The commercial alite was characterized, and the details are shown in Table 1 and Fig.1a. shows the X-ray fluorescence (XRF) measurement performed on the commercial alite with a Supermin200 instrument (Rangaku Corporation, Japan). The commercial alite powder was pressed into a flat pellet before the XRF test. The Ca/Si ratio of the raw material was measured to be 2.74, less than the theoretical value 3, indicating the presence of impurities. The crystalline composition of alite was analyzed by Quantitative X-ray Diffraction (Q-XRD). The results showed that the purity was about 89.3 wt.%, and the remaining phase was β-C_2S. The hydration products of C_3S and β-C_2S were similar.[27] β-C_2S would dissolve slowly as C_3S hydrated due to the higher solubility of C_3S.[28] So the impurity had limited on the hydration kinetics of C_3S at early ages. Fig. 1b shows the particle size distribution of alite powder measured on a Malvern MS3000 laser particle analyzer. The wet dispersion method was adopted in this study with isopropanol as the dispersing agent. Three repeated tests were conducted; each test lasted for 15 s. The string rate was set to be 3000 rpm. The average particle size (D[4,3]) is 13.1 μm. NaCl (NC), $MgCl_2$ (MC), and Na_2SO_4 (NS) are the main inorganic salts in seawater, according to ASTM D1141-98.[29] Therefore, in this study, the single salt (AR grade) solutions with the same concentration as those present in the ASTM standard (0.42 mol/L NC, 0.055 mol/L NS and 0.029 mol/L MC) were prepared and used.

Table 1 Oxide compositions of alite.

Composition	CaO	SiO_2	MgO	Al_2O_3	P_2O_5	SO_3	K_2O	Fe_2O_3	SrO	ZrO_2
wt.%	72.4	26.4	0.0866	0.912	0.114	0.0234	0.0473	0.0224	0.0142	0.0238

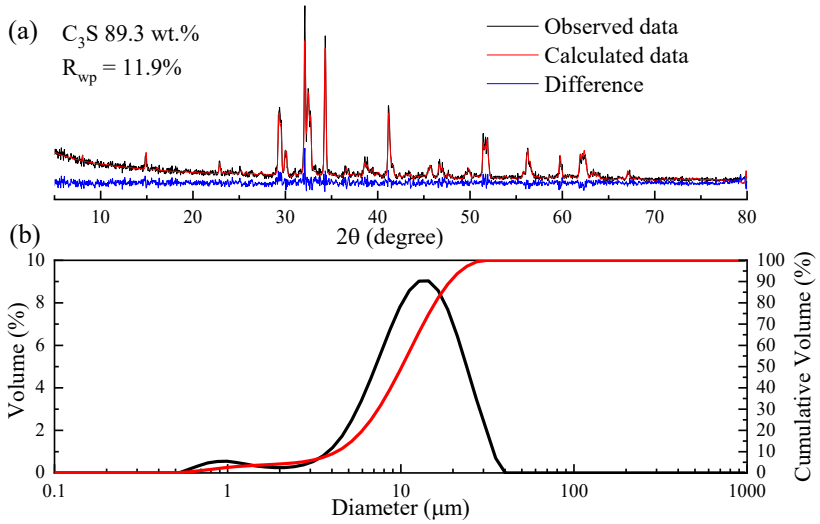

Fig. 1. (a) Crystalline phase compositions and (b) particle size distribution of alite used in this study.

Experimental procedures

In this study, the same high water-binder-ratio (10) was adopted as the previous study.[19] With such a high ratio, the complete reaction of alite would be promoted, and the hydration products could be easily characterized.[30]

For the isothermal calorimetry test, Samples of 5 g alite were mixed thoroughly with 50 g of the prepared salt solutions for 1 min by hand before the samples were put into the isothermal calorimeter (I-Cal 4000, Calmetrix), which was placed at room temperature of 20 ± 2℃. The measurement was monitored for 48 h.

Separately, alite was mixed thoroughly with deionized water (DI) and the different salt solutions at the same water-binder-ratio of 10. 2 g of alite was mixed with 20 g salt solutions in a plastic tube and the setups were shaken in an oscillator for 5 min before being stored in an N_2 filled container. After the selected curing period (6 h to 28 d), The samples were first centrifuged at 4000 rpm for 10 minutes, and then the separated solutions were filtered via 0.45 μm mixed cellulose esters membrane filters. The solid phase was washed with isopropanol twice for stopping further hydration, and to avoid the decomposition of hydration products due to the high temperature, the samples were dried in a vacuum desiccator at room temperature 20 ± 2℃ for 24 h for later testing.[31] The solutions were kept in a N_2 filled container before analysis.

Characterization techniques

For X-ray diffraction analysis (XRD Rigaku Smartlab), the powder samples were mixed with 20 wt.% α-Al_2O_3 (as internal standard) before characterization. The internal standard was mixed with the respective sample using a pestle and mortar gently to achieve better homogeneity and avoid over-grinding. The measurement was operated under the Bragg-Brentano geometry mode at 40 kV and 30 mA. The data collection range was 7° - 70° 2θ for CuKα radiation with a step size of 0.02° (0.5 s for each step). After collecting the data, the Rietveld method was used to quantify the phase compositions of the hydration products by GSAS II software.[32] The global refinement parameters for Rietveld refinement included in this study were background coefficients, sample displacement, phase scale factor, Lorentz polarisation factor, and cell parameters. The ICSD database was used in this study with the phases C_3S (ICSD no. 4331, space group P-1), C_2S (ICSD no. 81099, space group $P6_3/mmc$) , $Ca(OH)_2$ (ICSD no. 202220, space group P-3m), and Al_2O_3 (ICSD no. 77810, space group R-3c). The morphology development of the hydration products was studied by scanning electron microscopy (SEM, Tescan MAIA3) and transmission electron microscope (TEM, JEOL Model JEM-2100). Before SEM tests, the samples were coated with gold. In the TEM experiment, the hydrated alite samples were first ground into a powder and then immersed in ethanol. Ultrasonic dispersion was used as a pre-treatment. 1 mL of the suspension liquid was transferred on a carbon microgrid support membrane. Then, the morphologies of C-S-H were characterized. At the same time, (Energy-dispersive

X-ray spectroscopy) EDX measurement was used to analyze the elemental compositions of the amorphous C-S-H phase. To study the polymerization of the reaction products, ^{29}Si nuclei was scanned on a solid-state NMR spectrometer (JEOL ECZ 500MHZ). More than 2000 scans were conducted before getting the spectra, which were then deconvoluted, and the contents of different silicate tetrahedra phases were calculated. Inductively coupled plasma - optical emission spectrometry (ICP-OES, Spectro Blue) and Ion chromatography (IC, Thermo Scientific Dionex Integrion HPIC) were used to determine the ion concentrations of the collected filtrates after the hydration period. The filtrates were digested by concentrated nitric acid before testing.[33]

Thermodynamic modelling

Thermodynamic modelling was carried out using the Gibbs free energy minimization program (GEMS).[34-35] The effects of NaCl, Na_2SO_4 and $MgCl_2$ in the mixing water on the hydration of alite were studied. PSI-Nagra[36] and Cemdata 18[37] databases were adopted in this system. C-S-H is described by a solid solution of C-S-H-JenD, C-S-H-JenH, C-S-H-TobD, C-S-H-TobH and NaSiOH, as the end members modified from the C-S-H presented by D. Kulik.[38] The activities of different species were calculated from the measured total concentrations at respective temperatures using GEMS. The activity coefficient of aqueous species was calculated based on the built-in extended Debye-Hückel equation (Helgeson).[39] The activity correction is thought to be applicable for solutions with up to about 1 mol/L ionic strength. In the highest concentration NC solution, the ionic strength is 0.42 mol/L. The distance of closest approach was 3.67 for KOH, and the semi-empirical parameter was 0.123 for KOH at 25℃.

Results and discussion

Hydration kinetics of alite at the early age

The isothermal calorimetry test results for the early hydration of alite are shown in Fig. 2. In the initial period, the heat release in our study was higher than conventional alite pastes, with a maximum heat release of about 84 J/g within 1 h. That was due to more dissolution of alite in a higher amount of liquid. The starting point of the acceleration period was shifted to earlier ages with the addition of the salts. At about 3 h, the acceleration period of NC, NS and MC systems started to occur, while the starting time for DI system

was about 6 h. This indicates that the induction period for salt-added samples was shorter than the reference group. This was consistent with the acceleration effect of seawater[19] and indicated that all these three main salts in seawater would contribute to the acceleration effect. During the acceleration period, the reaction rate was different for each group. Overall, the reaction rates for the salt-added systems were higher compared to the reference DI system. The reaction rate of MC system was faster than the other groups before 4 h according to the cumulative heat release (Fig. 2b). At about 7.5 h, the NC group showed the highest reaction rate compared to other systems. The maximum reaction rate of DI system was far lower than the other systems.

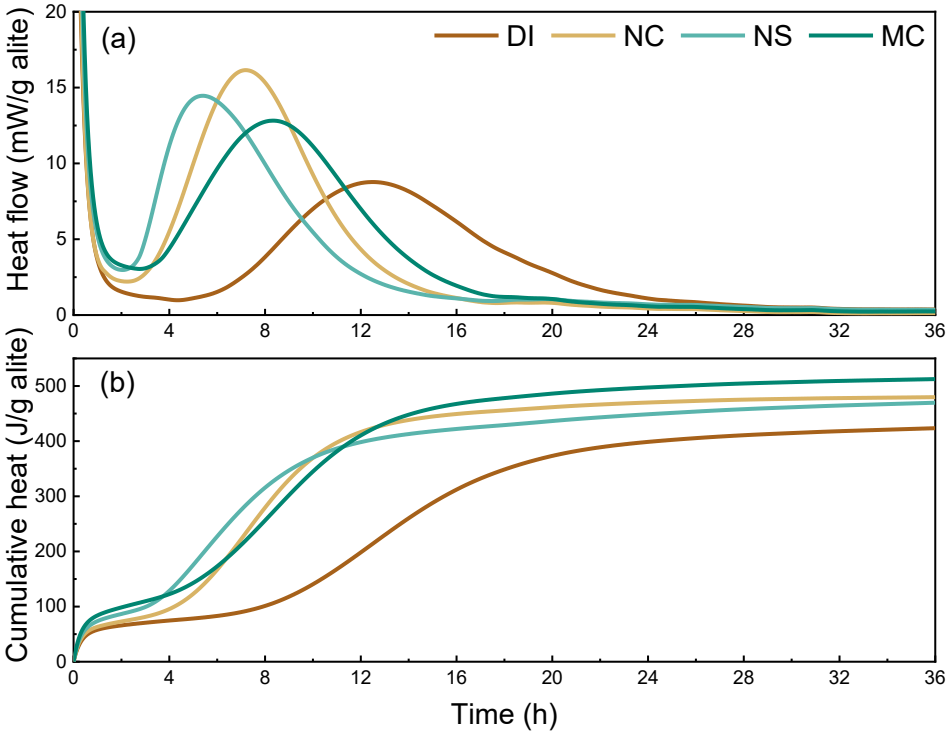

Fig. 2. (a) Heat flow and (b) Cumulative heat release for the alite pastes with the incorporation of varied salt.

At the same time, GEMS modelling was applied to study the solution and solid-phase composition as shown in Fig. 3. Before the end of the induction period, the primary reaction is the dissolution of alite into solution. In this period, calcium species (e.g. Ca^{2+}, $CaOH^{-}$)

were formed and continually increased as indicated by the GEMS modelling results (Fig. 3a). With the addition of the single salts, the induction period was shortened compared to DI system (Fig. 2a). This was due to the increasing dissolution rate of alite and the high calcium species concentration shown in Fig. 3a. At the same time, for DI and NC system, a small amount of C-S-H started to form. While for NS added system, there was $CaSO_4$ formed and dissolved in the solution.

Moreover, as the reaction progressed, gypsum started to precipitate before the formation of portlandite. That caused the early ending of the induction period compared to other systems. It was also why the cumulative heat release for NS system was higher than the NC system in the induction period. For MC systems, the early hydration products were M-S-H and brucite. Due to the severe heat release of brucite formation, the cumulative heat release of the MC system was the highest, as shown in Fig. 2b. However, portlandite formation was delayed. So, the induction period for the MC system was prolonged compared to NC and NS system. As the hydration progressed, the cumulative heat release for the MC system became the highest because a large amount of brucite was formed.

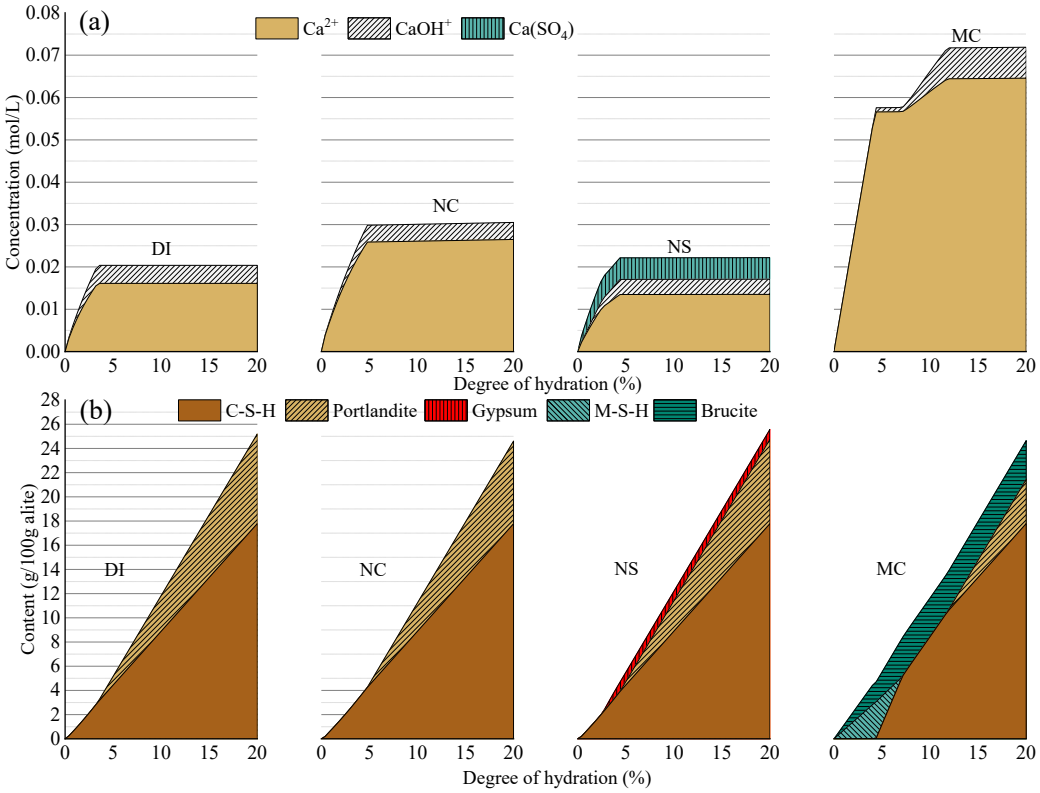

Fig. 3. GEMS modelling results for (a) the concentration of calcium species and (b) the solid phase composition.

Ion concentration variation in solutions

The changes in concentrations of different individual cations with time in the filtrates are shown in Fig. 4. The results showed that the dissolution of alite in the salt solution was accelerated by adding the individual seawater salts. The concentration of Ca species for the DI system was 0.016 ± 0.001 mol/L at 6 h and lower than those in salt added systems. That was consistent with the isothermal calorimetry test results and the GEMS modelling that at the early age of the hydration, alite dissolved quickly in the salt solutions and reached a higher Ca species concentration compared to DI system. As a result, the hydration rate was accelerated. As for the salt-added groups, the concentration of Ca species for NS system increased sharply to 0.066 ± 0.006 mol/L in the first 6 h, which was consistent with the early starting of the acceleration period. At the same time, gypsum was formed as detected by XRD results. As hydration proceeded, the concentration of Ca species decreased to a

level similar to that in DI. The concentration of Na species showed an inverse trend of the Ca species, that during the sharp increase of Ca species in the solution, the Na species decreased to 0.01 ± 0.001 mol/L at 6 h. While after 1 d, the concentration of Na species recovered to the initial level at around 0.050 mol/L. A similar trend can be seen in the results for the NC system, but the time to reach the maximum Ca species concentration (0.053 ± 0.002 mol/L) was about 12 h. As for Na species in the NC system, the concentration decreased to 0.058 ± 0.004 mol/L at 6 h, while after 1 d, the concentration recovered to about 0.41 mol/L. However, according to GEMS modelling (Fig. 6a), the concentrations of Na species for NC and NS systems remained at a stable value during the whole hydration process. That means the sharp decrease of Na species in the solution was not due to the formation of a stable new phase but to the surface complexation reaction[40-41] or the attraction by the surface charge[42-43]. So, at later ages, the Na species were rereleased to the solution, only resulting in a small reduction of the initial concentrations, consistent with the GEMS modelling. A noticeable trend was observed for the MC system, where the concentration of Ca species increased continually to 0.047 M before 1 d, after which it stabilized to a constant value, which was higher than any other system. At the same time, a large amount of Mg species was consumed, and the concentration of Mg species in the solution decreased from 0.055 M to almost zero after 6 h. That was due to the quick formation of brucite. Similar results were also obtained in the thermodynamic modelling (Fig. 3). The apparent increase of Ca species in the solution can be attributed to the leaching of portlandite, and the OH^- tends to combine with Mg species to form brucite.

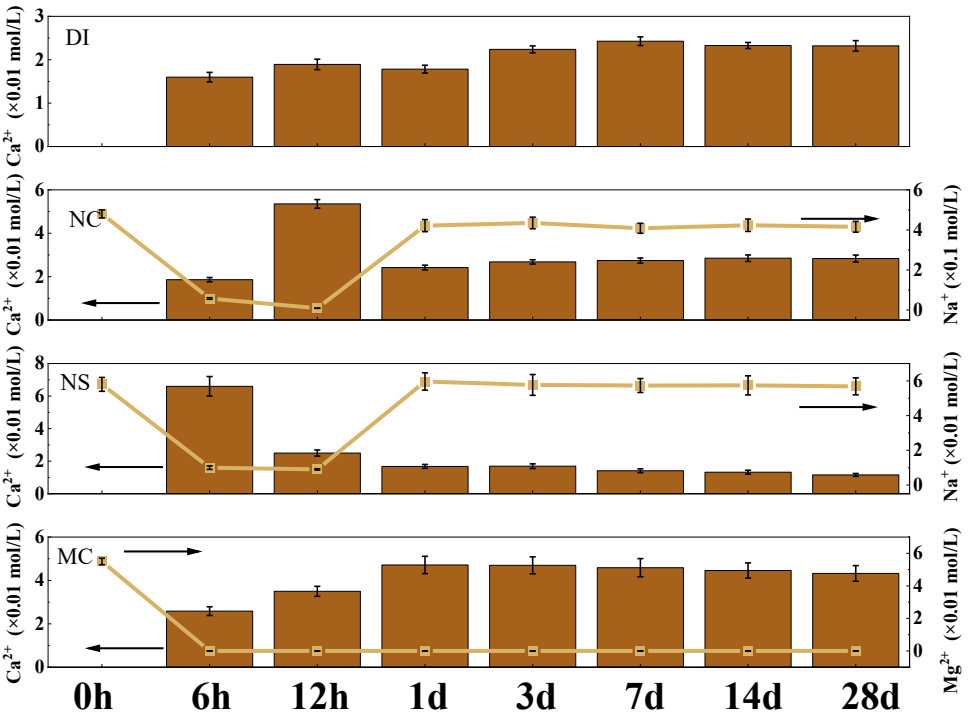

Fig. 4. Variation of cations in filtrates.

The variation of the anions with time is shown in Fig. 5. Both Cl species and S species concentrations decreased with time. The concentration of Cl species in the NC solution decreased from 0.42 mol/L at 0 h to 0.36 mol/L at 28d, while that for the MC group decreased from 0.11 mol/L to 0.04 mol/L. The level of reduction of Cl species concentration was similar for these two groups. However, according to the GEMS modelling, the concentrations of Cl species remained at a stable value, as shown in Fig. 6b. That indicates that the decrease of Cl species was mainly due to C-S-H absorption.[44-45] As for S species, the decrease trends are consistent between the test results and GEMS modelling because of the formation of gypsum.

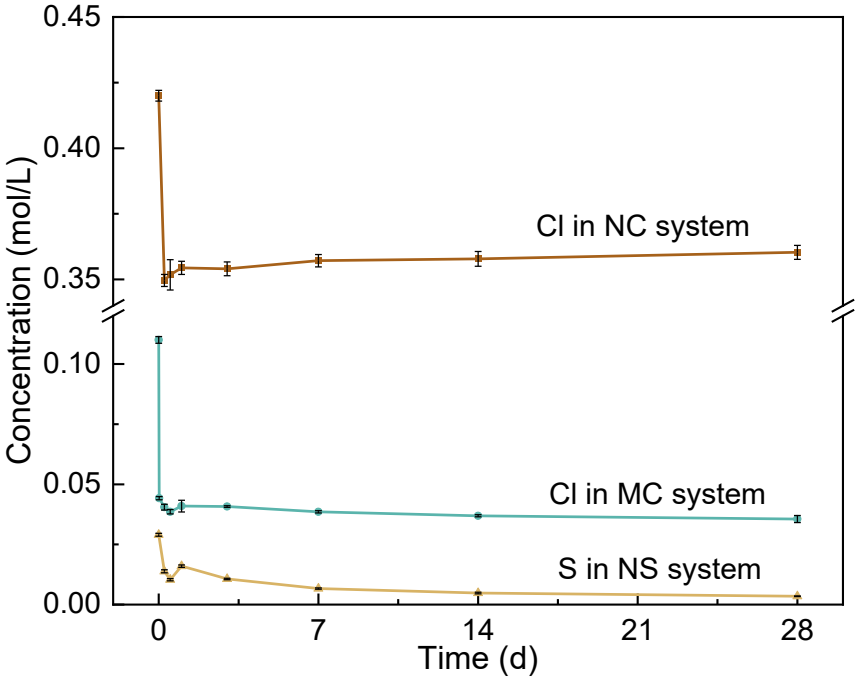

Fig. 5. Variation of anions in filtrates.

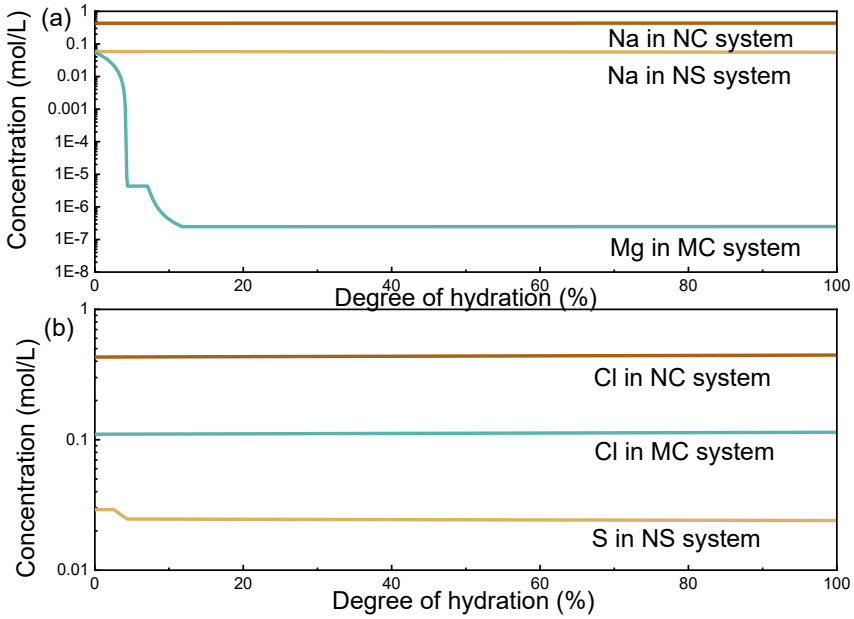

Fig. 6. GEMS modelling results for the concentrations of (a) cations and (b) anions in solutions.

Phase assemblages in hydration products

The phase assemblages in the hydration products were characterized by XRD tests as shown in Fig. 7. At 12 h the main hydration products for the DI system were portlandite and C-S-H. There was no new crystalline phase formed with the addition of NC. However, the addition of NS caused the formation of gypsum, which was consistent with the GEMS modelling results (Fig. 3b). For the MC system, because of the presence of Mg species, brucite was formed during the whole process of hydration. That caused the noticeable concentration decrement of Mg species in solutions, as shown in Fig. 4. The XRD tests results provide another evidence for GEMS modelling and the ion concentration variations results. With the addition of NC, no new phase was formed, but a higher concentration of Ca species was obtained in this system. So only the formation rate of C-S-H and portlandite was accelerated. For the NS system, because of the presence of S species, gypsum was formed as the hydration product and a part of it was dissolved in the solution. This also caused the increase of the Ca species concentration in the solution. This was found to be consistent with the previous study on alite pastes mixed with seawater. The abundant SO_4^{2-} in seawater would contribute to the formation of gypsum in alite pastes.[19] Brucite was found to be the main new hydration products in the MC system. Owing to the quick formation rate of brucite and the higher Ca species concentration limitation, the hydration of alite in the MC solution was accelerated.

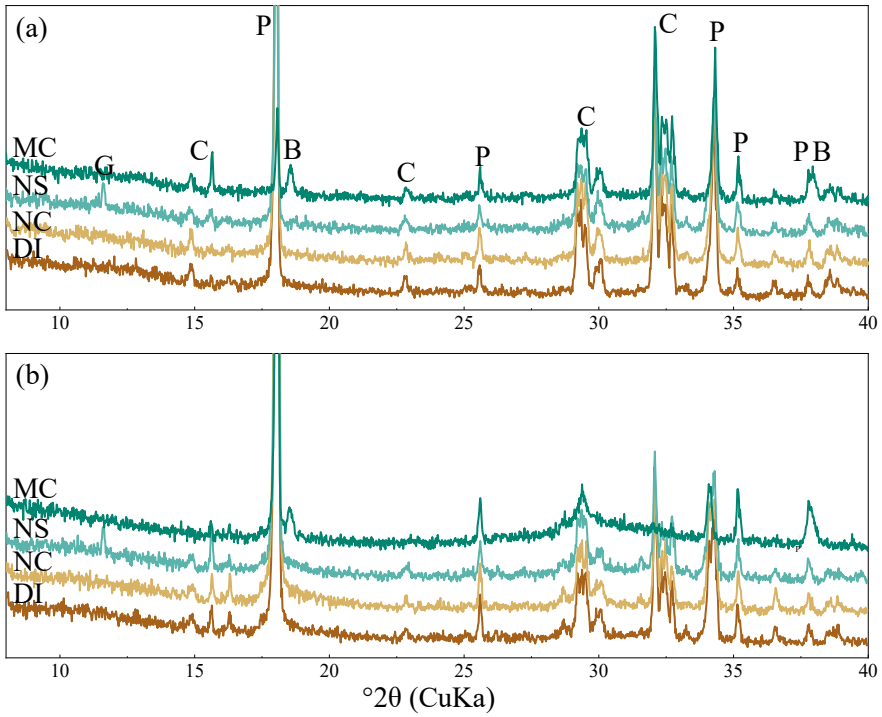

Fig. 7. XRD spectra of hydration products at (a) 12 h and (b) 28 d

(G: gypsum, C: C_3S, P: Portlandite, B: Brucite)

Besides the qualitative analysis of the XRD results as shown above. The Rietveld method was applied to calculate the amount of alite that remained after partial hydration in different salt solutions, as shown in Fig. 8. The degree of hydration (DoH) of alite can be calculated using Eq. 1, where P is the percentage of alite in the raw material and R is the remaining content of alite.

$$DoH = (P(alite) – R(alite)) / P(alite) * 100\% \quad (1)$$

The results show DoH of alite was enhanced with the addition of the single salts within 1 d, and about 40% of alite was hydrated within 6 h in the salt added solutions while the DoH for the DI water case was about 20%. The results were consistent with the calorimetry tests, as alite was still in its induction period in DI while the addition of the single salts contributed to the dissolution of alite and accelerated the hydration, leading to the early initiation of the acceleration period. At 28 d, most alite was consumed in all groups. It means that the salt solutions exerted their major impacts at an early age within 1 d. This

was consistent with the ion variation test results described and indicated that the dissolution rate of alite dominated the hydration rate of alite. It was noteworthy that the hydration kinetics of alite in dilute solutions was faster than that of alite pastes, so it still needed further study on the alite pastes with low water-binder-ratio.

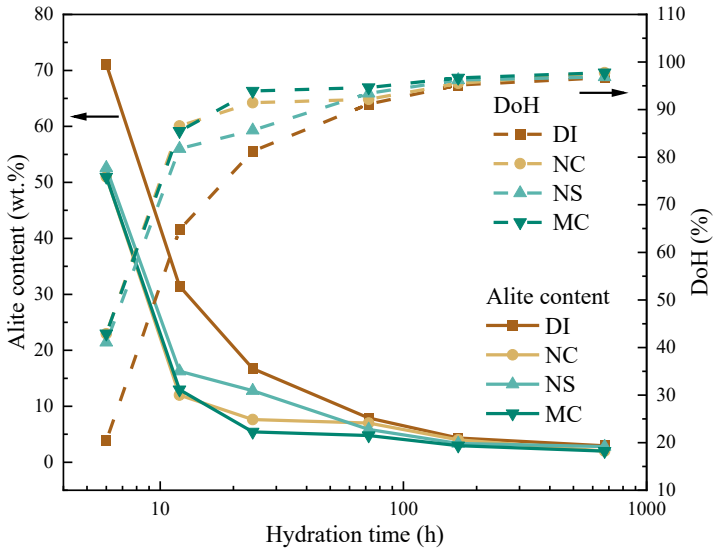

Fig. 8. Percentage of alite remained calculated by XRD-Rietveld method and DoH calculated according to alite consumption.

Morphology analysis

Considerable research results showed that C-S-H is formed in a fibrillar structure.[31, 46-47] Fig. 9 shows the TEM micrographs of the alite samples hydrated for 12 h. The needle-like fibrillar products were confirmed to be C-S-H gel by EDX results. Apart from the DI group, EDX showed the C-S-H was able to absorb a small portion of the cations and anions in the salt solution, which was the reason for the concentration of Na and Cl species decrease as shown in Fig. 4 and Fig. 5, but the GEMS modelling showed no apparent change. This is because the GEMS modelling can only model the chemical bonding of the hydration products, but part of anions is physically bound to hydration products in the actual results.[48-49] In the TEM images, the average length of C-S-H fibres was about 150 nm, while the average C-S-H fibre lengths of salt added systems were over 200 nm. That

is caused by the faster hydration rate of alite at early ages. The longer C-S-H fibres in the salt-added solutions contributed to a looser structure. This was also verified by the SEM results (Fig. 10). As for the composition of early hydration products, the Ca/Si ratio of C-S-H in DI was significantly higher than that of other groups because, for DI system, there were mainly inner C-S-H around the alite particles, which have a higher Ca/Si ratio. For salt-added systems, more outer C-S-H formed, which caused the reduction of the measured Ca/Si ratio. The penetration depth of the electron in the EDX test was about 2 μm.[50] Thus, the Ca/Si ratio calculated results might be slightly higher due to the intermix of C-S-H with anhydrous phase and portlandite. To weaken this effect, we chose the region mainly occupied with C-S-H.

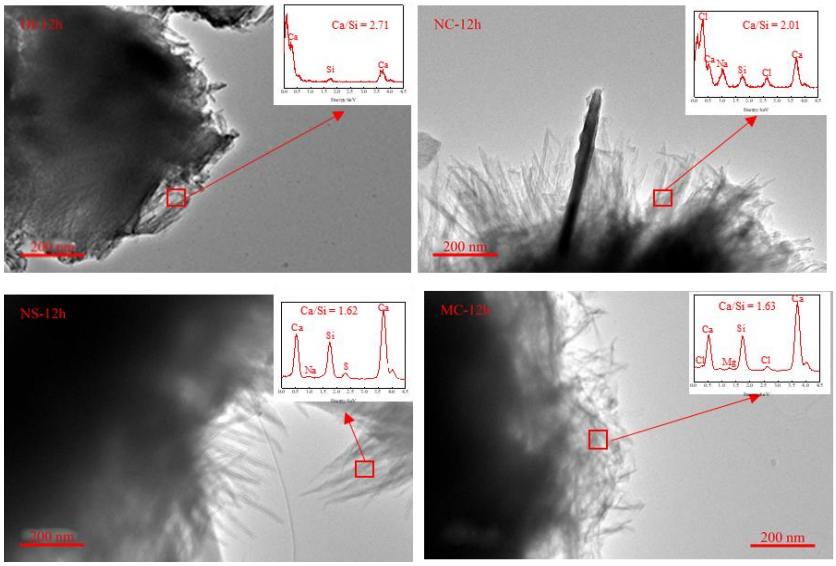

Fig. 9. Morphology and EDX analysis of C-S-H at 12 h in TEM.

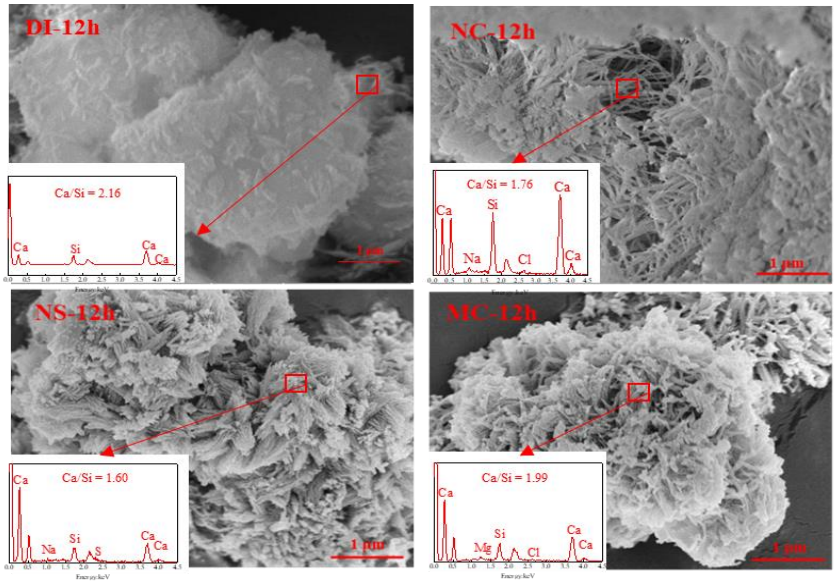

Fig. 10. Morphology and EDX analysis of C-S-H at 12 h in SEM.

To study the single salts' effects on the morphology of C-S-H at later ages, the morphology of the hydration products at 28 d was characterized. Fibrillar C-S-H grew together to form plates and foil-like clusters, as shown in Fig. 11 and Fig. 12. Both TEM and SEM showed the Ca/Si ratio was about 1.5 except for the MC group, where the ratio was slightly lower. That was due to the co-presence of C-S-H and brucite. TEM results (Fig. 11) showed that the later hydration product in DI was a more compact foil-like matrix. In comparison, although the matrix of the hydration products in the salt-added groups was looser in the TEM image, as shown in Fig. 12, the SEM images showed no apparent difference between the different groups of samples. The fibres formed in the early hydration merged. As a result, thicker fibres and plates were observed. Since high water-binder-ratio was adopted in this study, more space was available for C-S-H to grow than alite pastes. That might affect the morphology development of C-S-H. Thus, the morphology evolution of alite pastes would be investigated in further studies.

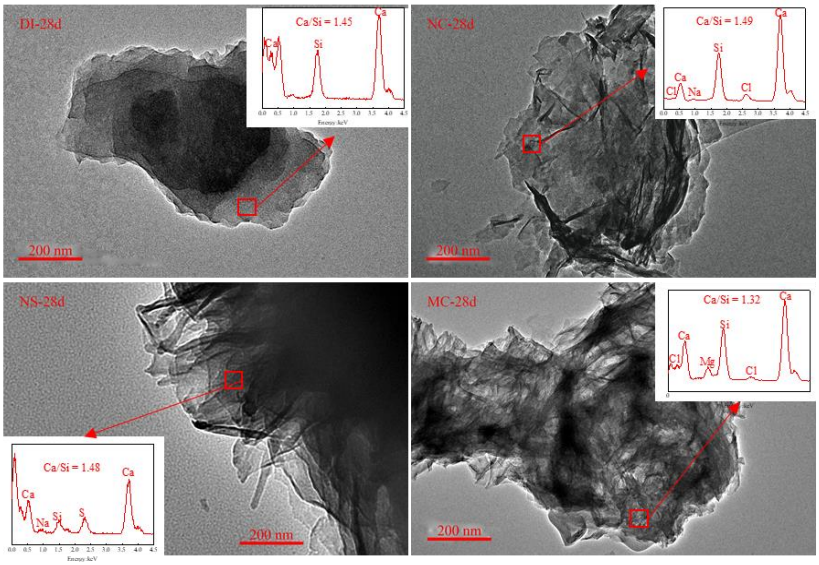

Fig. 11. Morphology and EDX analysis of C-S-H at 28 d in TEM.

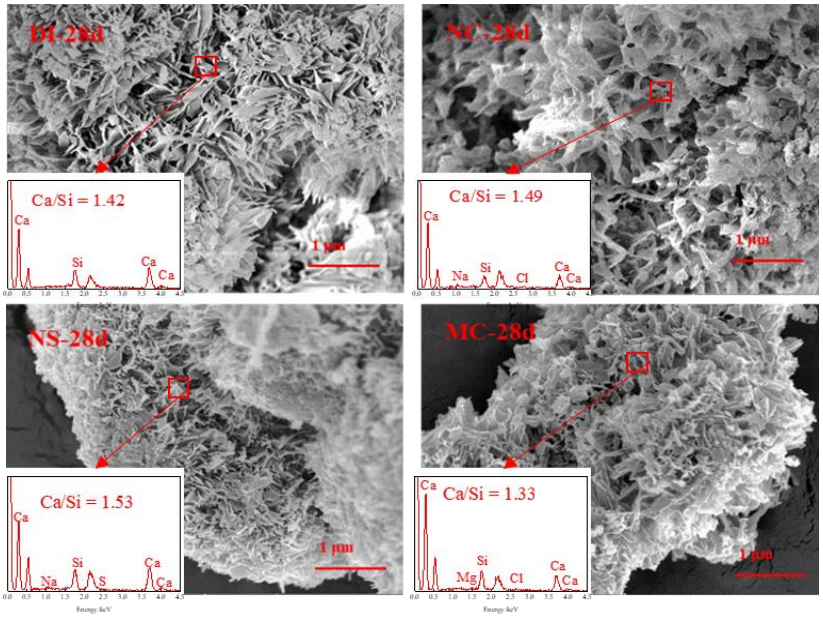

Fig. 12. Morphology and EDX analysis of C-S-H at 28 d in SEM.

^{29}Si solid-state MAS NMR

The deconvolution results of the acquired ^{29}Si MAS NMR spectra of the samples hydrated for 6 h and 28 d are shown in Fig. 13. The NMR results can provide information on the amount of Q^n, where n indicates the number of bridging oxygen atoms around one Si atom,[51] and for example, alite has nine Q^0 positions because of the different crystal

structures in the range -60 to -75 ppm.[52] Fig. 13a shows that, besides the Q^0 peaks, there are also two more peaks at around -79 and -85 ppm, corresponding to Q^1 and Q^2 units formation in C-S-H gels. Q^1 denotes two conditions: the end silica tetrahedra for a C-S-H chain or the silica tetrahedra in a dimer and Q^2 represents the interchain silica tetrahedra in C-S-H gel.[53]

The NMR spectra were deconvoluted to calculate the mean chain lengths (MCL), and polymerization degrees (PD) by using Eqs. 2 to 3 and the results are shown in Table 2.

$$MCL = 2 \times (Q^1 + Q^2) / Q^1 \quad (2)$$

$$PD = Q^2 / Q^1 \quad (3)$$

Table 2 ^{29}Si MAS NMR spectrum analysis.

Paste	Q^n/%			MCL	PD
	Q^0	Q^1	Q^2		
DI-6h	88.6	11.4	0.0	2	0
NC-6h	21.3	51.7	27.0	3.04	0.52
NS-6h	36.1	55.9	8.0	2.29	0.14
MC-6h	43.1	44.9	12.0	2.53	0.26
DI-28d	0.0	61.6	38.4	3.25	0.62
NC-28d	0.0	68.2	31.8	2.93	0.47
NS-28d	0.0	63.8	36.2	3.13	0.57
MC-28d	0.0	66.7	33.3	2.99	0.49

Fig. 13a and Table 2 show that Q^1 and Q^2 were more predominant in the salt-added groups compared with the reference group. For the DI water group, there was no Q^2 detected, and this suggested a predominant C-S-H dimer structure. That was the initial status of the early formed C-S-H. Less Q^0 and a higher percentage of Q^2 in salt-added

groups indicated the fast hydration of alite and the quick polymerization of C-S-H. Since Q^0 only existed in alite and C_2S. The higher polymerization of C-S-H also caused the longer fibres observed in the TEM tests. These results were also consistent with the calorimetry test result, where the addition of single salt contributed to the alite dissolution and the polymerization of hydration products. As a result, the MCL and PD of DI system were lower than that of the salt-added systems at the early age.

At 28d, most of the alite was hydrated. The polymerization degree and the mean chain length decreased with the addition of the single salts. However, the difference of MCL at 28 d was not as evident as that at 6 h. That could be the reason why no significant morphology change was detected in the TEM and SEM testings.

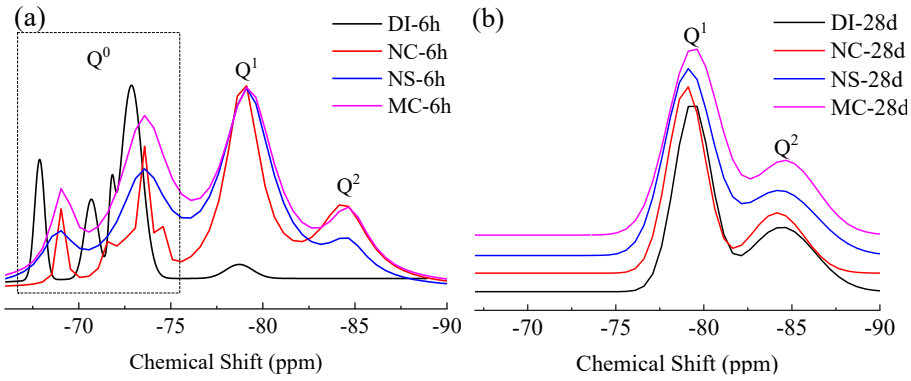

Fig. 13. ^{29}Si MAS NMR spectra of (a) 6h and (b) 28d samples.

At the early period of hydration, the main reaction driving process was the dissolution of alite and polymerization of silicates. The silicates in alite were isolated in the Q^0 status. As the hydration proceeded, silicates tended to combine to form the chain structure, and more Q^1 and Q^2 were found in the NMR results. Since the salt-added samples hydrated faster than DI samples, the polymerization of the salt-added groups was higher, contributing to the growth of C-S-H fibres and producing longer and thinner fibres, as indicated by Fig. 9 and Fig. 10. That caused the formation of a looser structure and facilitated the ion exchange between alite and the hydration solutions. This also contributed to the faster hydration reaction.

After almost complete hydration of alite at 28 d, the structure of C-S-H tended to be stable. However, the polymerization degree and average chain length of C-S-H were reduced with the addition of the single salts. The depolymerization of the silicate chain mechanism is likely due to the excessive Ca species present in the salt solutions, which is verified by both the Ion concentration test and the GEMS modelling. As shown in Fig. 14, the larger amount of Ca Species in salt solutions would cause the breaking of the silicate chain of the C-S-H structure.[54-55] As a result, the long silicate chain would be divided into several short chains. Since the MCL of C-S-H did not change significantly at 28 d, no noticeable morphology difference was observed. The found plates and foil-like clusters were associated with the merging of C-S-H fibres.

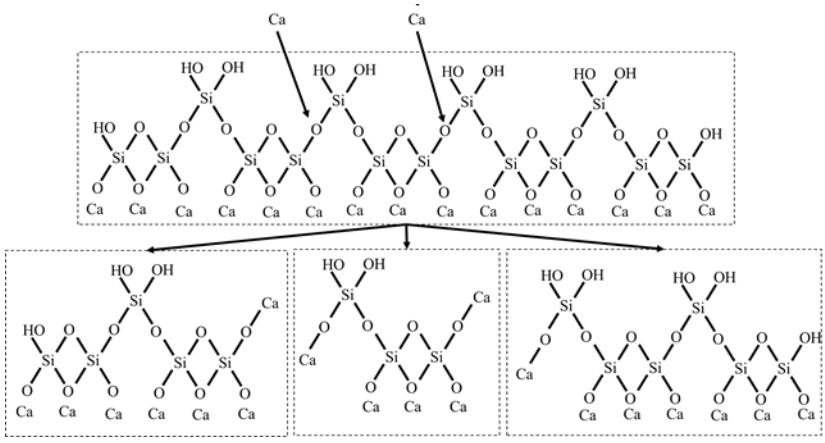

Fig. 14. The Schematic for the breaking of silicate chain by Ca^{2+}.

Conclusion

Alite was hydrated in DI water and three soluble salt solutions (NaCl, Na_2SO_4, $MgCl_2$) to understand the effects of the common salts in seawater on hydration. Based on the results of this study, the following conclusions can be drawn:

- The addition of the single salts was observed to increase the Ca species concentration in the solution compared to the DI system, contributing to the formation of portlandite and C-S-H. Thus, higher early age hydration rates were obtained for the salt systems.

- In the Na_2SO_4 system, gypsum was characterized as the new hydration product. While for the $MgCl_2$ system, brucite formed quickly in a short period, consuming a large amount of Mg species in the solution.
- At the early age of hydration, the C-S-H fibres around alite grew faster in the salt solutions than DI, causing a looser microstructure and facilitating ion exchanges. This was another reason for accelerating the hydration. However, no noticeable difference in C-S-H morphology between the DI and salt solution samples was detected at the age of 28 days.
- The polymerization degree of C-S-H in the salt-added systems was lower than that of the DI system due to the excessive Ca species present in solutions.

Acknowledgement

The work described in this paper was supported by a grant from the Research Grants Council of the Hong Kong Special Administrative Region, China (Project No. T22-502/18-R).

References

(1) Statista. Cement production in the United States and worldwide from 2010 to 2020. https://www.statista.com/statistics/219343/cement-production-worldwide/#statisticContainer (accessed 2021-06-29).
(2) Kummu, M.; Guillaume, J.; de Moel, H.; Eisner, S.; Flörke, M.; Porkka, M.; Siebert, S.; Veldkamp, T. I.; Ward, P. J. The world's road to water scarcity: shortage and stress in the 20th century and pathways towards sustainability. *Scientific reports* **2016,** *6*, 38495.
(3) Guo, M.; Hu, B.; Xing, F.; Zhou, X.; Sun, M.; Sui, L.; Zhou, Y. Characterization of the mechanical properties of eco-friendly concrete made with untreated sea sand and seawater based on statistical analysis. *Constr. Build. Mater.* **2020,** *234*, 117339.
(4) Li, Y.; Zhao, X.; Singh, R. R.; Al-Saadi, S. Experimental study on seawater and sea sand concrete filled GFRP and stainless steel tubular stub columns. *Thin-Walled Structures* **2016,** *106*, 390-406.
(5) Wang, J.; Liu, E.; Li, L. Multiscale investigations on hydration mechanisms in seawater OPC paste. *Constr. Build. Mater.* **2018,** *191*, 891-903.
(6) Ragab, A. M.; Elgammal, M. A.; Hodhod, O. A.; Ahmed, T. E. Evaluation of field concrete deterioration under real conditions of seawater attack. *Constr. Build. Mater.* **2016,** *119*, 130-144.
(7) Shang, B.; Li, Y. Application feasibility of HRB400 steel in seawater and marine sand concrete. *Mater. Corros.* **2018,** *69* (10), 1478-1488.

(8) Uthaman, S.; George, R.; Vishwakarma, V.; Harilal, M.; Philip, J. Enhanced seawater corrosion resistance of reinforcement in nanophase modified fly ash concrete. *Constr. Build. Mater.* **2019,** *221*, 232-243.
(9) Zhou, A.; Qin, R.; Chow, C. L.; Lau, D. Structural performance of FRP confined seawater concrete columns under chloride environment. *Compos. Struct.* **2019,** *216*, 12-19.
(10) Wang, Z.; Zhao, X.; Xian, G.; Wu, G.; Raman, R. S.; Al-Saadi, S.; Haque, A. Long-term durability of basalt-and glass-fibre reinforced polymer (BFRP/GFRP) bars in seawater and sea sand concrete environment. *Constr. Build. Mater.* **2017,** *139*, 467-489.
(11) Guo, F.; Al-Saadi, S.; Raman, R. S.; Zhao, X. Durability of fiber reinforced polymer (FRP) in simulated seawater sea sand concrete (SWSSC) environment. *Corros. Sci.* **2018,** *141*, 1-13.
(12) Robert, M.; Benmokrane, B. Combined effects of saline solution and moist concrete on long-term durability of GFRP reinforcing bars. *Constr. Build. Mater.* **2013,** *38*, 274-284.
(13) Jackson, M. D.; Moon, J.; Gotti, E.; Taylor, R.; Chae, S. R.; Kunz, M.; Emwas, A. H.; Meral, C.; Guttmann, P.; Levitz, P. Material and elastic properties of Al-tobermorite in ancient Roman seawater concrete. *J. Am. Ceram. Soc.* **2013,** *96* (8), 2598-2606.
(14) Younis, A.; Ebead, U.; Suraneni, P.; Nanni, A. Fresh and hardened properties of seawater-mixed concrete. *Constr. Build. Mater.* **2018,** *190*, 276-286.
(15) Xiao, J.; Qiang, C.; Nanni, A.; Zhang, K. Use of sea-sand and seawater in concrete construction: Current status and future opportunities. *Constr. Build. Mater.* **2017,** *155*, 1101-1111.
(16) Li, Q.; Geng, H. N.; Huang, Y.; Shui, Z. H. Chloride resistance of concrete with metakaolin addition and seawater mixing: A comparative study. *Constr. Build. Mater.* **2015,** *101*, 184-192.
(17) Dhondy, T.; Remennikov, A.; Shiekh, M. N. Benefits of using sea sand and seawater in concrete: a comprehensive review. *Aust. J. Struct. Eng.* **2019,** *20* (4), 1-10.
(18) Li, P.; Li, W.; Yu, T.; Qu, F.; Tam, V. W. Investigation on early-age hydration, mechanical properties and microstructure of seawater sea sand cement mortar. *Constr. Build. Mater.* **2020,** *249*, 118776.
(19) Yaseen, S. A.; Yiseen, G. A.; Poon, C. S.; Li, Z. Influence of Seawater on the Morphological Evolution and the Microchemistry of Hydration Products of Tricalcium Silicates (C_3S). *ACS Sustain. Chem. Eng.* **2020,** *8* (42), 15875-15887.
(20) Edwards, G.; Angstadt, R. The effect of some soluble inorganic admixtures on the early hydration of portland cement. *J. Appl. Chem.* **1966,** *16* (5), 166-168.
(21) Kondo, R.; Daimon, M.; Sakai, E.; Ushiyama, H. Influence of inorganic salts on the hydration of tricalcium silicate. *J. Chem. Technol. Biotechnol* **1977,** *27* (1), 191-197.
(22) Wilding, C.; Walter, A.; Double, D. A classification of inorganic and organic admixtures by conduction calorimetry. *Cem. Concr. Res.* **1984,** *14* (2), 185-194.
(23) Bullard, J. W.; Jennings, H. M.; Livingston, R. A.; Nonat, A.; Scherer, G. W.; Schweitzer, J. S.; Scrivener, K. L.; Thomas, J. J. Mechanisms of cement hydration. *Cem. Concr. Res.* **2011,** *41* (12), 1208-1223.
(24) Scrivener, K. L.; Juilland, P.; Monteiro, P. J. M. Advances in understanding hydration of Portland cement. *Cem. Concr. Res.* **2015,** *78*, 38-56.
(25) Juilland, P.; Gallucci, E.; Flatt, R.; Scrivener, K. Dissolution theory applied to the induction period in alite hydration. *Cem. Concr. Res.* **2010,** *40* (6), 831-844.
(26) Brown, P. W.; Harner, C. L.; Prosen, E. J. The effect of inorganic salts on tricalcium silicate hydration. *Cem. Concr. Res.* **1986,** *16* (1), 17-22.
(27) Thomas, J. J.; Ghazizadeh, S.; Masoero, E. Kinetic mechanisms and activation energies for hydration of standard and highly reactive forms of β-dicalcium silicate (C2S). *Cem. Concr. Res.* **2017,** *100*, 322-328.
(28) Scrivener, K. L.; Nonat, A. Hydration of cementitious materials, present and future. *Cem. Concr. Res.* **2011,** *41* (7), 651-665.
(29) ASTM International. *Standard Practice for the Preparation of Substitute Ocean Water*: ASTM D1141-98: West Conshohocken, PA, **2013**. DOI: 10.1520/D1141-98R13

(30) Zhang, L.; Yamauchi, K.; Li, Z.; Zhang, X.; Ma, H.; Ge, S. Novel understanding of calcium silicate hydrate from dilute hydration. *Cem. Concr. Res.* **2017,** *99*, 95-105.
(31) Mota, B.; Matschei, T.; Scrivener, K. The influence of sodium salts and gypsum on alite hydration. *Cem. Concr. Res.* **2015,** *75*, 53-65.
(32) Toby, B.; Madden, T.; Suchomel, M.; Baldwin, J.; Von Dreele, R. A scanning CCD detector for powder diffraction measurements. *J. Appl. Crystallogr.* **2013,** *46* (4), 1058-1063.
(33) He, P.; Zhang, B.; Lu, J.-X.; Poon, C. S. ASR expansion of alkali-activated cement glass aggregate mortars. *Constr. Build. Mater.* **2020,** *261*, 119925.
(34) Kulik, D. A.; Wagner, T.; Dmytrieva, S. V.; Kosakowski, G.; Hingerl, F. F.; Chudnenko, K. V.; Berner, U. R. GEM-Selektor geochemical modeling package: revised algorithm and GEMS3K numerical kernel for coupled simulation codes. *Computational Geosciences* **2013,** *17* (1), 1-24.
(35) Wagner, T.; Kulik, D. A.; Hingerl, F. F.; Dmytrieva, S. V. GEM-Selektor geochemical modeling package: TSolMod library and data interface for multicomponent phase models. *The Canadian Mineralogist* **2012,** *50* (5), 1173-1195.
(36) Hummel, W.; Berner, U.; Curti, E.; Pearson, F.; Thoenen, T. Nagra/PSI chemical thermodynamic database 01/01. *Radiochimica Acta* **2002,** *90* (9-11), 805-813.
(37) Lothenbach, B.; Kulik, D. A.; Matschei, T.; Balonis, M.; Baquerizo, L.; Dilnesa, B.; Miron, G. D.; Myers, R. J. Cemdata18: A chemical thermodynamic database for hydrated Portland cements and alkali-activated materials. *Cem. Concr. Res.* **2019,** *115*, 472-506.
(38) Kulik, D. A. Improving the structural consistency of CSH solid solution thermodynamic models. *Cem. Concr. Res.* **2011,** *41* (5), 477-495.
(39) Helgeson, H. C.; Kirkham, D. H.; Flowers, G. C. Theoretical prediction of the thermodynamic behavior of aqueous electrolytes by high pressures and temperatures; IV, Calculation of activity coefficients, osmotic coefficients, and apparent molal and standard and relative partial molal properties to 600 degrees C and 5kb. *AmJS* **1981,** *281* (10), 1249-1516.
(40) Viallis, H.; Faucon, P.; Petit, J.; Nonat, A. Interaction between salts (NaCl, CsCl) and calcium silicate hydrates (C−S−H). *J. Phys. Chem. B* **1999,** *103* (25), 5212-5219.
(41) Viallis-Terrisse, H.; Nonat, A.; Petit, J.-C. Zeta-potential study of calcium silicate hydrates interacting with alkaline cations. *J. Colloid Interface Sci.* **2001,** *244* (1), 58-65.
(42) Lothenbach, B. Thermodynamic equilibrium calculations in cementitious systems. *Mater. Struct.* **2010,** *43* (10), 1413-1433.
(43) Labbez, C.; Nonat, A.; Pochard, I.; Jönsson, B. Experimental and theoretical evidence of overcharging of calcium silicate hydrate. *J. Colloid Interface Sci.* **2007,** *309* (2), 303-307.
(44) Divet, L.; Randriambololona, R. Delayed ettringite formation: the effect of temperature and basicity on the interaction of sulphate and CSH phase. *Cem. Concr. Res.* **1998,** *28* (3), 357-363.
(45) Nachbaur, L.; Nkinamubanzi, P.-C.; Nonat, A.; Mutin, J.-C. Electrokinetic Properties which Control the Coagulation of Silicate Cement Suspensions during Early Age Hydration. *J. Colloid Interface Sci.* **1998,** *202* (2), 261-268.
(46) Juenger, M.; Monteiro, P.; Gartner, E.; Denbeaux, G. A soft X-ray microscope investigation into the effects of calcium chloride on tricalcium silicate hydration. *Cem. Concr. Res.* **2005,** *35* (1), 19-25.
(47) Peterson, V. K.; Juenger, M. C. G. Hydration of tricalcium silicate: effects of $CaCl_2$ and sucrose on reaction kinetics and product formation. *Chem. Mater.* **2006,** *18* (24), 5798-5804.
(48) Yogarajah, E.; Nawa, T.; Kurumisawa, K. Influence of Surface Electrical Properties of C–S–H on Chloride Binding in Slag-Blended Cementitious Materials. *J. Mater. Civ. Eng* **2018,** *30*, 04018064.
(49) Friedmann, H.; Amiri, O.; Aït-Mokhtar, A. Physical modeling of the electrical double layer effects on multispecies ions transport in cement-based materials. *Cem. Concr. Res.* **2008,** *38* (12), 1394-1400.

(50) Chen, J. J.; Sorelli, L.; Vandamme, M.; Ulm, F. J.; Chanvillard, G. A Coupled nanoindentation/SEM-EDS study on low water/cement ratio Portland cement paste: evidence for C–S–H/Ca (OH) 2 nanocomposites. *J. Am. Ceram. Soc.* **2010,** *93* (5), 1484-1493.
(51) Vega, A. J.; Scherer, G. W. Study of structural evolution of silica gel using ^{1}H and ^{29}Si NMR. *J. Non-Cryst. Solids* **1989,** *111* (2-3), 153-166.
(52) Sánchez-Herrero, M. J.; Fernández-Jiménez, A.; Palomo, A. C_3S and C_2S hydration in the presence of Na_2CO_3 and Na_2SO_4. *J. Am. Ceram. Soc.* **2017,** *100* (7), 3188-3198.
(53) Wang, J.; Han, B.; Li, Z.; Yu, X.; Dong, X. Effect investigation of nanofillers on CSH gel structure with Si NMR. *J. Mater. Civ. Eng.* **2019,** *31* (1), 04018352.
(54) Lothenbach, B.; Nonat, A. Calcium silicate hydrates: Solid and liquid phase composition. *Cem. Concr. Res.* **2015,** *78*, 57-70.
(55) Mendoza, O.; Giraldo, C.; Camargo, S. S.; Tobón, J. I. Structural and nano-mechanical properties of Calcium Silicate Hydrate (C-S-H) formed from alite hydration in the presence of sodium and potassium hydroxide. *Cem. Concr. Res.* **2015,** *74*, 88-94.

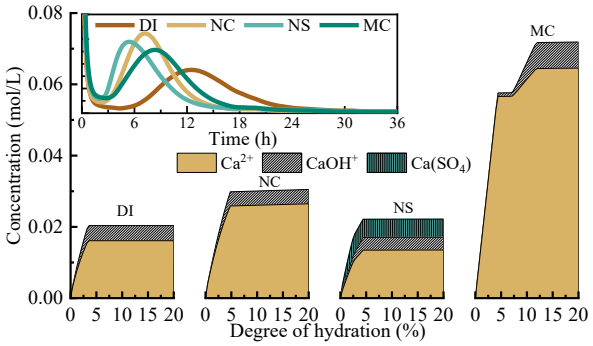

The main inorganic salts in seawater increase the saturated Ca concentrations in solutions, contributing to the hydration of alite. This research will help the usage of seawater in construction as a sustainable material.